Research Paper

Changes in audiometric threshold and frequency selectivity correlate with cochlear histopathology in macaque monkeys with permanent noise-induced hearing loss

Jane A. Burton[a], Chase A. Mackey[a], Kaitlyn S. MacDonald[b], Troy A. Hackett[b], Ramnarayan Ramachandran[b],*

[a] *Neuroscience Graduate Program, Vanderbilt University, Nashville, TN 37235, United States*
[b] *Department of Hearing and Speech Sciences, Vanderbilt University Medical Center, Nashville, TN 37232, United States*

ARTICLE INFO

ABSTRACT

Exposure to loud noise causes damage to the inner ear, including but not limited to outer and inner hair cells (OHCs and IHCs) and IHC ribbon synapses. This cochlear damage impairs auditory processing and increases audiometric thresholds (noise-induced hearing loss, NIHL). However, the exact relationship between the perceptual consequences of NIHL and its underlying cochlear pathology are poorly understood. This study used a nonhuman primate model of NIHL to relate changes in frequency selectivity and audiometric thresholds to indices of cochlear histopathology. Three macaques (one *Macaca mulatta* and two *Macaca radiata*) were trained to detect tones in quiet and in noises that were spectrally notched around the tone frequency. Audiograms were derived from tone thresholds in quiet; perceptual auditory filters were derived from tone thresholds in notched-noise maskers using the rounded-exponential fit. Data were obtained before and after a four-hour exposure to a 50-Hz noise centered at 2 kHz at 141 or 146 dB SPL. Noise exposure caused permanent audiometric threshold shifts and broadening of auditory filters at and above 2 kHz, with greater changes observed for the 146-dB-exposed monkeys. The normalized bandwidth of the perceptual auditory filters was strongly correlated with audiometric threshold at each tone frequency. While changes in audiometric threshold and perceptual auditory filter widths were primarily determined by the extent of OHC survival, additional variability was explained by including interactions among OHC, IHC, and ribbon synapse survival. This is the first study to provide within-subject comparisons of auditory filter bandwidths in an animal model of NIHL and correlate these NIHL-related perceptual changes with cochlear histopathology. These results expand the foundations for ongoing investigations of the neural correlates of NIHL-related perceptual changes.

© 2020 Elsevier B.V. All rights reserved.

1. Introduction

Hearing impairment causes significant perceptual deficits across the frequency and time domains (e.g. Moore, 1995). These deficits have been studied for decades using psychophysical measures in humans and animal models in order to quantify the perceptual changes underlying the global hearing difficulties reported by hearing impaired patients. Temporal and frequency resolution are impaired for many patients with hearing loss (e.g. Florentine et al., 1980; Hall and Grose, 1989; Moore, 1985, 1995; Reed et al., 2009),

with the degree of impairment often being related to severity of hearing loss. While quantifying these behavioral impairments helps guide appropriate treatment and rehabilitation strategies, the identification of specific underlying cochlear damage and associated neural changes provides an additional therapeutic target and helps elucidate the variability in rehabilitative success.

The link between auditory perception and indices of cochlear histopathology has been examined in animal models of ototoxicity, age-related hearing loss, and noise-induced hearing loss. Many of these studies were conducted in small-animal models (e.g. chinchilla: Ward and Duvall, 1971; Clark and Bohne, 1978; Ryan et al., 1979, Hamernik et al., 1989; cat: Miller et al., 1963; see early review by Saunders et al., 1991), and there is a comparatively smaller literature in nonhuman primates (reviewed in Burton et al., 2019). Most of this work was limited to examinations of audiometric thresholds, with little characterization of higher level auditory

* Corresponding author.
E-mail addresses: jane.a.burton@vanderbilt.edu (J.A. Burton), chase.mackey@vanderbilt.edu (C.A. Mackey), kaitlyn.s.macdonald@vanderbilt.edu (K.S. MacDonald), troy.a.hackett@vanderbilt.edu (T.A. Hackett), ramnarayan.ramachandran@vanderbilt.edu (R. Ramachandran).

perceptual characteristics (however, see Radziwon et al., 2019). Systematic studies using the macaque model are relatively new and may serve as a bridge between the rodent and human literatures on noise-induced hearing loss (NIHL).

Our laboratory previously established a model of NIHL in macaque monkeys (Valero et al., 2017; Hauser et al., 2018). The macaque NIHL model provides the advantages of a close phylogenetic relationship to humans, thorough knowledge of the history of noise exposure, the ability to successfully complete complex listening tasks, and the opportunity to utilize more invasive neuroscientific methodologies such as single-unit neurophysiology and post-mortem cochlear histology and neuroanatomy (Burton et al., 2019). Noise overexposure to a narrowband stimulus resulted in frequency-specific but variable loss across subjects of outer hair cells (OHCs), inner hair cells (IHCs), and inner hair cell ribbon synapses (Valero et al., 2017). This anatomical damage was accompanied by perceptual deficits as measured by elevated tone detection thresholds in quiet, decreased threshold shift rates during masked tone detection, and decreased release from masking during tone detection in sinusoidally amplitude modulated noise masker (Hauser et al., 2018). The characterization of this NIHL model is extended here to examine perceptual frequency selectivity measured using the notched-noise method in noise-exposed macaques. The aims of this study were 1) to examine the relationship between severity of noise-induced hearing loss and loss of frequency selectivity and 2) to examine the relationship between indices of cochlear histopathology as measured by OHC, IHC, and ribbon synapse survival and loss of hearing sensitivity and frequency selectivity. To the best of the authors' knowledge, this is the first report of perceptual auditory filters in an animal model of NIHL.

2. Methods

Experiments were conducted on one male rhesus macaque (*Macaca mulatta*, Monkey L, ten years old at the time of noise exposure) and two male bonnet macaques (*Macaca radiata*, Monkey E and G, eleven and nine years old at the time of exposure, respectively), as well as a cohort of non-exposed male control subjects with normal hearing sensitivity (*Macaca mulatta*, n = 5, 6–10 years old). Macaques were maintained on a 12:12-h light:dark cycle and all procedures occurred between 8 AM and 6 PM during their light cycle. Monkeys E and G were socially housed; however, all other subjects were individually housed, per incompatibility for social housing as identified by repeated behavioral assessments. The macaques had visual, auditory, and olfactory contact with conspecifics maintained within the housing room, as well as daily visual, auditory, or olfactory supplemental enrichment. All procedures were approved by the Animal Care and Use Committee at the Vanderbilt University Medical Center and were in strict compliance with the National Institutes of Health guidelines for animal research.

Experiments were conducted in sound treated booths (Industrial Acoustics Corp, NY; Acoustic Systems, Austin, TX). During the task, monkeys sat in an acrylic primate chair that was custom designed for comfort and with no obstruction to sounds on either side of their heads (Audio chair, Crist Instrument Co., Hagerstown, MD). Monkeys were head-fixed via a surgically-implanted titanium head holder and trained to perform a Go/No-Go lever release task using fluid reward as positive reinforcement (for details about surgical preparation and behavioral task, see Dylla et al., 2013; Burton et al., 2018a). The monkey's head was fixed to the chair such that the head and ears directly faced the center of a loudspeaker at a distance of 36 inches. The loudspeaker (SA1 loudspeaker, Madisound, WI) and amplifier (SLA2, Applied Research Technologies, Rochester, NY) were able to deliver sounds between

50 Hz and 40 kHz. Calibration using a 1/4" probe microphone (model 378C01, PCB Piezotronics Inc., Depew, NY) placed at the approximate entrance of the subjects' ear canals revealed that the output of the speakers varied by approximately ±3 dB across the frequency range. Tones and noise were delivered from the same loudspeaker.

2.1. Noise exposure

The details of the noise exposure matched those in in Valero et al. (2017) and Hauser et al. (2018). Briefly, the monkeys were treated with atropine (0.04 mg/kg) and sedated with a mixture of ketamine (10–15 mg/kg) and midazolam (0.05 mg/kg IM) prior to intubation. Sedation was maintained with 1–2% isoflurane and vital signs were monitored throughout the procedure. The noise exposure was conducted in a sound treated booth (Acoustic Systems, Austin, TX) while the monkey was lying prone on a table with the head slightly elevated. Closed-field loudspeakers (MF1, Tucker-Davis Technologies) were coupled to the subject's ears using 10 cm long PE tubing and pediatric ER-3A insert earphones that were trimmed and deeply inserted into each ear canal. A 50-Hz band of noise centered at 2 kHz was presented simultaneously to both ears via the insert earphones for four hours.

Monkey L was exposed at 141 dB SPL and Monkeys E and G were exposed at 146 dB SPL. This design allowed us to examine changes in frequency selectivity with varying degrees of hearing impairment and cochlear damage. The level of the exposure stimulus varied by less than 0.3 dB SPL over the course of the four-hour procedure. The monkeys were monitored intensively for a minimum of 72 h post-procedure. Auditory brainstem responses and distortion product otoacoustic emissions were measured in separate sedated procedures pre- and post-exposure to supplement behavioral measures of hearing impairment (for further details, see Hauser et al., 2018).

2.2. Behavioral task

The behavioral task was identical to the methods described in Burton et al. (2018a). Briefly, the monkeys were trained to detect tones in quiet or embedded in noise maskers. To initiate a trial, the monkey pressed down on a lever (Model 829 Single Axis Hall Effect Joystick, P3America, San Diego, CA). After a variable hold time, a signal (tone, 80% of trials) or catch trial (no tone, 20% of trials) was presented. Upon correct lever release on signal trials, the monkey received a fluid reward. If the monkey did not release the lever during a signal trial, this was taken to indicate non-detection, and no reward or penalty was administered. Lever release on catch trials resulted in a timeout penalty.

The experiments were controlled by a computer running OpenEx software (System 3, TDT Inc., Alachua, FL). Within each block, tone sound pressure levels spanned a 60 dB range and were randomly interleaved with catch trials. Flat spectrum broadband noise was generated from a uniform distribution and band-limited to 40 kHz. In experiments using masking noise, the level was constant at 50 dB SPL.

2.2.1. Tone detection in quiet

Pre- and post-exposure audiograms for each monkey were determined from tone detection performance in quiet, as reported previously (Hauser et al., 2018). Signal frequencies of 0.125, 0.25, 0.5, 1, 1.414, 2, 2.828, 4, 8, 16, and 32 kHz were chosen to span the audible range of macaques (Pfingst et al., 1978; Dylla et al., 2013) in octave steps with additional resolution near the noise exposure band. Audiograms were obtained prior to noise exposure and serial audiograms were obtained over the course of several weeks
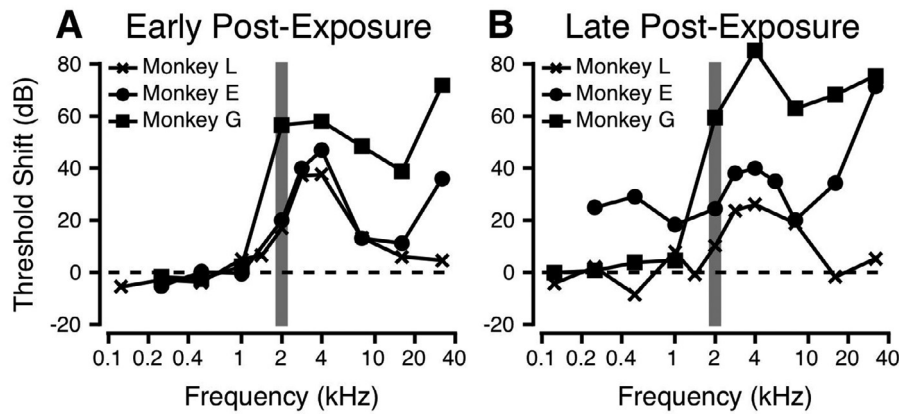
Fig. 1. Audiometric threshold shift (dB) plotted as a function of frequency (kHz) for Monkey L (×), Monkey E (○), and Monkey G (□). Threshold shift was calculated as (post-exposure threshold – pre-exposure threshold). A. Early post-exposure threshold shifts collected a minimum of 5 weeks after the noise exposure and just prior to frequency selectivity data collection. B. Late post-exposure threshold shifts collected just prior to euthanasia (Monkey L and E) or at a later time point several months after frequency selectivity data collection (Monkey G).

following noise exposure. Audiometric threshold shifts at each frequency were quantified by taking the difference between the post-exposure and pre-exposure tone detection thresholds in quiet at that frequency.

Here, we report audiometric threshold shifts from two post-exposure timepoints. The first set of audiometric threshold shifts were obtained a minimum of 5 weeks after the subject's noise exposure and just prior to collection of the data used to estimate frequency selectivity (Fig. 1A; "Early Post-Exposure"). Post-exposure frequency selectivity data were not collected until a minimum of 60 days after the exposure, well after initial temporary threshold shifts had stabilized.

The second set of post-exposure audiometric thresholds were obtained following frequency selectivity data collection (Fig. 1B; "Late Post-Exposure"). Due to the large behavioral task sets for each subject and variable completion rates for each task, post-exposure survival times were variable across subjects. Unexpectedly, we observed extensive changes in audiometric thresholds throughout post-exposure survival for two of the three subjects (Monkeys E and G). Late post-exposure audiometric thresholds were collected within one month of euthanasia for Monkeys L and E. Audiometric thresholds could not be obtained at a later time point for Monkey G, due to limited behavioral performance and likely profound deafness in the mid to high frequencies.

2.2.2. Tone detection in notched-noise masker

Modeled after Patterson and Nimmo-Smith (1980) and Glasberg et al. (1984b), the notched-noise methods used here were similar to those described in Burton et al. (2018a). In brief, tone detection performance was measured in the presence of two 50 dB SPL narrowband noise maskers (bandwidth = $0.4*f_0$) placed symmetrically and asymmetrically around the tone frequency. Signal frequencies (f_0) were 0.5, 1, 1.414, 2, 2.828, 4, 8, and 16 kHz. (Note: 32 kHz was not tested due to bandwidth limitations of the speaker, which prevented the upper notched-noise bands from being presented at the specified level.) The normalized half notch widths ($\Delta f/f_0$) of the symmetric noise notches were 0.0, 0.05, 0.1, 0.2, 0.3, 0.5, 0.6, 0.65, and 0.8. Upward and downward shifted asymmetric notches were generated by shifting the high frequency edge of the lower band of noise $0.2f_0$ closer or farther from f_0, respectively, while maintaining a particular notch width ($\Delta f/f_0$ = 0.3, 0.4, 0.5, 0.6, 0.65, and 0.8). Detection performance was measured and filters estimated pre-exposure and beginning a minimum of 60 days after noise exposure.

2.3. Calculation of behavioral thresholds

Behavioral performance was analyzed according to signal detection theoretic methods, as described in Dylla et al. (2013), Bohlen et al. (2014), and Burton et al. (2018a). Briefly, at each tone level (*level*), hit rate was calculated ($H(level)$) based on the proportion of releases on trials with the tone at that sound level. False alarm rate (FA) was calculated based on the proportion of releases on catch trials. Based on signal detection theory, $H(level)$ and FA were then converted into units of standard deviation of a standard normal distribution (*z-score*, norminv in MATLAB) to estimate d' according to $d'(level) = z(H(level)) - z(FA)$ (Macmillan and Creelman, 2005). Because we wanted these results to serve as a baseline for neurophysiological studies where we would measure (noise) and (signal+noise) representation distributions, we converted the Yes/No analysis to a 2-alternative forced choice analysis and calculated the behavioral accuracy at each tone level using the probability correct (*pc*) metric as follows: $pc(level) = z^{-1}(d'(level)/2)$. Here, the inverse z transform (z^{-1}) converts a unique number of standard deviations of a standard normal distribution into a probability correct (normcdf in MATLAB). The conversion of d' to the *pc* measure was to facilitate the comparison of psychometric functions with neurometric functions obtained from neuronal responses using distribution free methods. The traditional threshold estimated at $d'=1$ corresponds to $pc(level)=0.76$.

The psychometric functions were fitted with a modified Weibull cumulative distribution function (cdf) according to $pc(level)_{fit} = c - d * e^{-(\frac{level}{\lambda})^k}$, where *level* was the tone level (in dB SPL), λ represents the threshold parameter and k corresponds to the slope parameter. c represents the saturation probability correct, and d was the estimate of chance performance. Threshold was calculated from the fit as the tone level that resulted in a pc_{fit} value of 0.76.

2.4. Filter shape and bandwidth analyses

Assuming that each side of the auditory filter was a rounded exponential, estimates of filter shape were obtained from the tone detection thresholds as a function of notch width, as reported in Burton et al. (2018a). Briefly, asymmetric filter estimates were obtained using the default settings in the publicly available ROEX3 program, developed by Moore and Glasberg. The rounded exponential (roex) filter shape is described by: $W(g) = (1 - r) * (1 + p * g) * e^{-p*g} + r$, where g is the normalized deviation from the tone frequency ($g = \Delta f/f_0$), and p and r are adjustable parameters. A larger value of p indicates a larger slope and there-

fore a narrower filter. For asymmetric filters, p_l and p_u are used to describe the lower and upper sides of the filter, respectively. r corresponds to the shallow tail of the filter. The $W(g)$ filter parameter values were iteratively adjusted in the software so as to achieve the smallest RMS difference between the predicted and actual threshold values.

Equivalent rectangular bandwidths were calculated from the p_l and p_u values, according to Glasberg et al. (1984b): $ERB(f_0) = f_0 * (2/p_l + 2/p_u)$. Change in frequency selectivity with hearing impairment was quantified according to the ratio: $ERB_{post-exposure}(f_0)/ERB_{baseline}(f_0)$.

2.5. Cochlear histological preparation and quantification

Histology and imaging were performed using procedures detailed previously (Valero et al., 2017). Briefly, following completion of the behavioral assays, animals were euthanized by an overdose of sodium pentobarbital (130 mg/kg), followed immediately by transcardial perfusion (2 l 0.9% phosphate-buffered saline, PBS; 2 l 4% phosphate-buffered paraformaldehyde, PFA). The round and oval windows were opened, cochleas perfused through the scala tympani with PFA, submerged in PFA for 2 h, then transferred to 0.12 M EDTA for decalcification.

Decalcified cochleas were dissected into quarter turns to obtain epithelial whole mounts of the organ of Corti containing the hair cells and most of the osseous spiral lamina at each location from base to apex. Immunohistochemistry was used to label pre-synaptic ribbons (mouse IgG1 anti-CtBP2 (C-terminal binding protein 2); BD Transduction Labs; 1:200); ii) glutamate receptor patches (mouse IgG2 anti-GluA2; Millipore; 1:200), iii) hair cell cytoplasm (rabbit anti-myo7a (myosin VIIa); Proteus Biosciences; 1:200), and iv) cochlear afferent and efferent fibers (chicken anti-NFH (neurofilament-H); Chemicon; 1:1000). Tissue was incubated in species-appropriate fluorescent secondary antibody conjugates (AlexaFluor) for secondary detection.

The tissue was imaged on a Leica SP8 confocal microscope, using a 63X glycerol objective (1.3 N.A.), to acquire 3-dimensional image stacks at each of 8 octave-spaced positions along the cochlear spiral from 0.125 to 32 kHz, with half-octave spacing in regions of significant hair cell loss. The frequency correlate of each image stack was computed from a cochlear frequency map based on a Greenwood function (Greenwood, 1990), assuming an upper frequency limit of 45 kHz. OHC, IHC, and ribbon synapse counts were averaged across two adjacent stacks for each cochlear place. Amira software (Visage Imaging) was used to quantify IHC afferent synapses from confocal z-stacks by identification of thresholded CtBP2-labeled puncta within hair cells. Normative ribbon synapse counts (per IHC) were defined as the mean count within non-exposed ears for each frequency region. Synapse counts from the exposed cochleas were compared to the normative values to determine percentage synapse survival along the cochlear length. Hair cell survival was assessed in low-power confocal z-stacks by counting cuticular plates normalized to the expected number of hair cells within each row.

2.6. Statistical analyses

All statistical analyses were completed in MATLAB (2018a; Mathworks Inc.). One-sample *t*-tests were used to compare post-exposure *ERB* values for each subject to mean *ERB* values compiled from pre-exposure and control macaques across different tone frequencies. Bonferroni corrections were applied to adjust for multiple comparisons. Specifically, *p*-values of 0.05, 0.01, and 0.001 were adjusted to 0.0023, 4.55×10^{-4}, and 4.55×10^{-5}, respectively, since twenty-two comparisons were completed.

Using the "fitlm" and "fitnlm" functions in MATLAB, simple linear regressions and exponential nonlinear regressions were applied to the normalized ERB (ERB/f_0) by absolute audiometric threshold data (Fig. 6A) to compare with previous literature. All data points were included in each regression analysis. The best model was determined according to the lowest Bayesian information criterion (BIC) value, which adds a penalty for the number of model parameters in order to avoid overfitting. These same analyses were completed for data comparing the ERB ratio and audiometric threshold shift (Fig. 6B), and for data comparing OHC, IHC, and ribbon synapse survival with audiometric threshold shift (Fig. 8) and *ERB* ratio (Fig. 9). Finally, stepwise multivariate linear regression models ("stepwiselm", with and without interactions included) were used to describe the relationship between audiometric threshold shift or *ERB* ratio with frequency and indices of cochlear histopathology (OHC, IHC, and ribbon synapse survival). This model fitting procedure systematically removes factors and interaction terms that do not add significant explanatory power to the model. The "plotResiduals" function was used to assess whether linear regressions were appropriate for use in the models.

In an attempt to provide the most legitimate comparisons, we used audiometric threshold shift data from two post-exposure timepoints (see Section 2.2.1) in the following ways: 1) audiometric threshold shifts from the early post-exposure timepoint were compared to frequency selectivity metrics due to the close relationship in time and 2) audiometric threshold shifts from the late post-exposure timepoint were compared to the indices of cochlear histopathology (OHC, IHC, and ribbon synapse survival) due to their closer relationship in time. While regressions between the frequency selectivity data and cochlear histology are inconvenienced by a long and variable time delay between behavioral data collection and cochlear harvesting, we believe that this represents a conservative comparison that still provides meaningful insight into the relationship between cochlear integrity and a facet of auditory perception.

3. Results

3.1. Tone detection in quiet

Tone detection in quiet was assessed before and after noise exposure in order to assess the degree of permanent hearing impairment. Fig. 1A shows audiometric threshold shifts for the three noise-exposed subjects, roughly 5 weeks post-exposure and just prior to measurement of frequency selectivity ("Early Post-Exposure"). Significant threshold shifts were observed at and above the center frequency of the exposure band (grey box; 2 kHz), as reported in Hauser et al. (2018). Threshold shifts were similar for Monkeys L and E and greatest for Monkey G, even though both Monkeys G and E were exposed at 146 dB SPL, and Monkey L was exposed at 141 dB SPL. All monkeys showed a peak in threshold shift roughly one half octave above the exposure band, which is similar to the high frequency, notched configuration observed in humans with noise-induced hearing loss (Gelfand, 2009). Both monkeys exposed at the higher level showed a second peak in their threshold shift patterns at the highest frequency tested. This extreme basal peak, while tonotopically inappropriate given the exposure band, is typical of permanent threshold shifts after acute exposures (e.g. Moody et al., 1978).

Audiometric thresholds were monitored for 7 to 27 months post-exposure (Fig. 1B; "Late Post-Exposure"). While the general patterns remained similar, the severity of threshold shift increased for the two cases exposed at 146 dB SPL (Monkeys E and G). Such ongoing threshold shifts are consistent with reports of accelerated age-related audiometric shifts in mice and humans with NIHL (Fernandez et al., 2015; Gates et al., 2000). Due to this change in
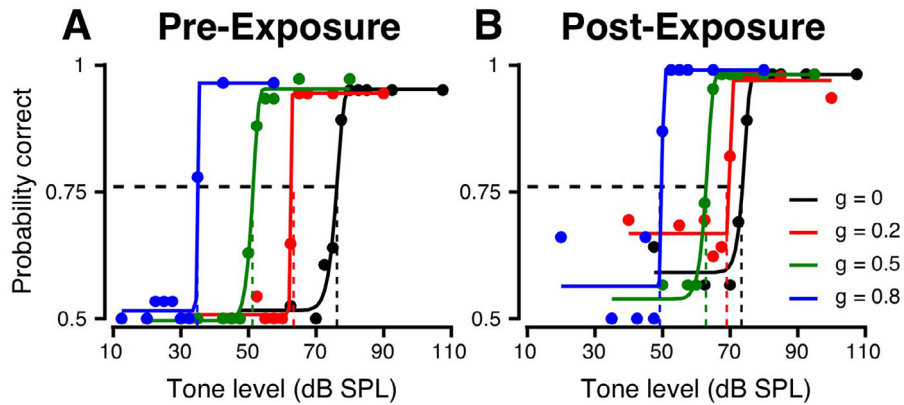
Fig. 2. Psychometric functions for the detection of tones in notched noise. A: Psychometric functions for detection of a 2.828 kHz tone in a 50 dB SPL/Hz masker in a normal hearing macaque (Monkey L, pre-exposure). Lines of different colors represent various g values. g-values shown are 0 (black), 0.2 (red), 0.5 (green), and 0.8 (blue). B: Similar to A, but following noise exposure at 141 dB SPL for 4 h (Monkey L, post-exposure). In both panels, horizontal dashed line represents $pc = 0.76$, and the vertical lines represent the tone levels required to evoke such performance. (For interpretation of the references to color in this figure legend, the reader is referred to the web version of this article.)

audiometric thresholds over time, each timepoint was utilized for different comparisons, as outlined in Section 2.6.

3.2. Auditory filters

Tone detection thresholds in notched-noise maskers were obtained from psychometric functions (Fig. 2). Prior to noise exposure (Fig. 2A), tone detection threshold (dashed line) decreased with increasing notch width ($g = \Delta f/f_0$; normalized deviation from the tone frequency) as expected (e.g. Patterson and Nimmo-Smith, 1980; Burton et al., 2018a). Post-exposure, at frequencies with significant threshold elevation (such as 2.828 kHz, Fig. 2B), thresholds decreased less for the same increase in notch width. At the same frequency and notch widths, Monkey G (with the poorest tone in quiet thresholds) also had higher masked thresholds than Monkey L and E.

Fig. 3 compares pre- and post-exposure thresholds in notched-noise maskers centered around different tone frequencies, plotted as a function of g value. As reported previously, pre-exposure threshold vs. g functions had negative slopes (Fig. 3A–C) (Burton et al., 2018a). Post-exposure (Fig. 3D–F), these functions were usually shallower for frequencies $\geq$ 2 kHz (red lines). In particular, the 2–8 kHz functions were nearly flat post-exposure, suggesting broader filters after damage.

Perceptual auditory filters obtained using asymmetric notches are shown in Fig. 4 for each subject before and after noise exposure. Pre-exposure, relative filter bandwidths (Fig. 4A–C) decreased with increasing tone frequency, consistent with previous reports (e.g. Moore and Glasberg, 1987; Burton et al., 2018a). Post-exposure, filters appear unchanged at frequencies < 2 kHz (Fig. 4D–F; black) and were generally broader at frequencies $\geq$ 2 kHz (Fig. 4D–F; red), except at 16 kHz for Monkey L and at 8 and 16 kHz for Monkey E.

To quantify filter shapes, the equivalent rectangular bandwidth (ERB) was measured (Fig. 5A and Table 1). Pre-exposure, ERB values increased with increasing frequency, consistent with previous reports in other species and in macaques (e.g. Humans: Glasberg and Moore, 1986; Macaques: Burton et al., 2018a; Marmosets: Osmanski et al., 2013; Chinchilla: Niemiec et al., 1992). Post-exposure ERB values (Fig. 5A, red lines) were significantly greater (i.e. broader tuning) at most frequencies above the exposure band, when compared to five normal-hearing macaques (Fig. 5A, black, mean and standard deviation; see Table 2 for one-sample t-test statistics).
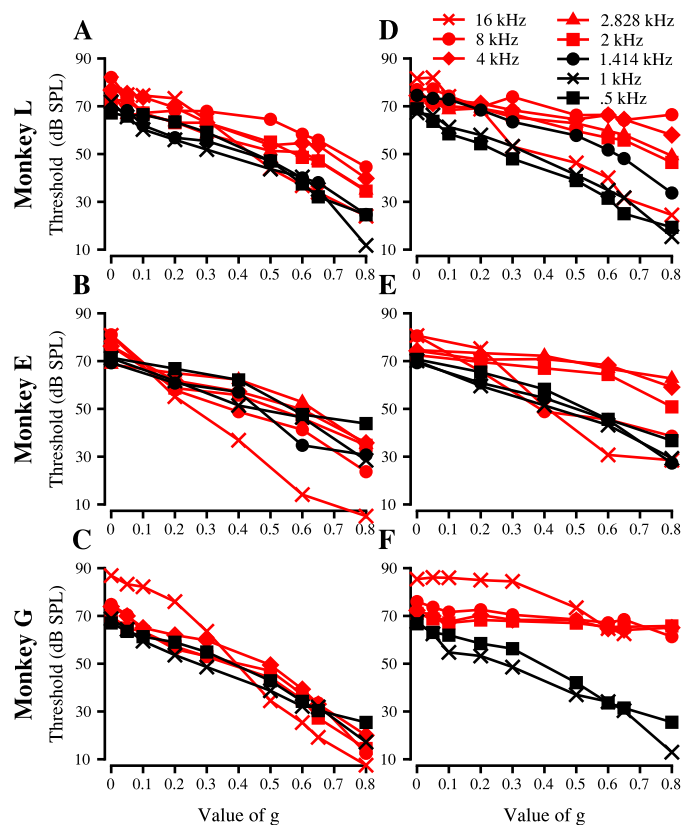
Fig. 3. Threshold (in dB SPL) as a function of g, the normalized notch width. A–C: Pre-exposure data for Monkey L, E, and G, respectively. D–F: Post-exposure data for Monkey L, E, and G, respectively. Frequencies below the noise exposure band are shown in black (0.5 kHz: □, 1 kHz: ×, 1.414 kHz: ○). Frequencies at and above the noise exposure band are shown in red (2 kHz: □, 2.828 kHz: △, 4 kHz: ◇, 8 kHz: ○, 16 kHz: ×). (For interpretation of the references to color in this figure legend, the reader is referred to the web version of this article.)

The ERB ratio (post-exposure ERB/pre-exposure ERB) allows for within-subject normalization, with values > 1 indicating broader filters post-exposure. Plotting ERB ratios (red in Fig. 5B) with the audiometric threshold shifts from Fig. 1A (grey in Fig. 5B) shows that filter bandwidths were wider at frequencies with larger threshold shifts, consistent with previous reports in humans (e.g. Tyler et al., 1984; Glasberg and Moore, 1986; Desloge et al., 2012).
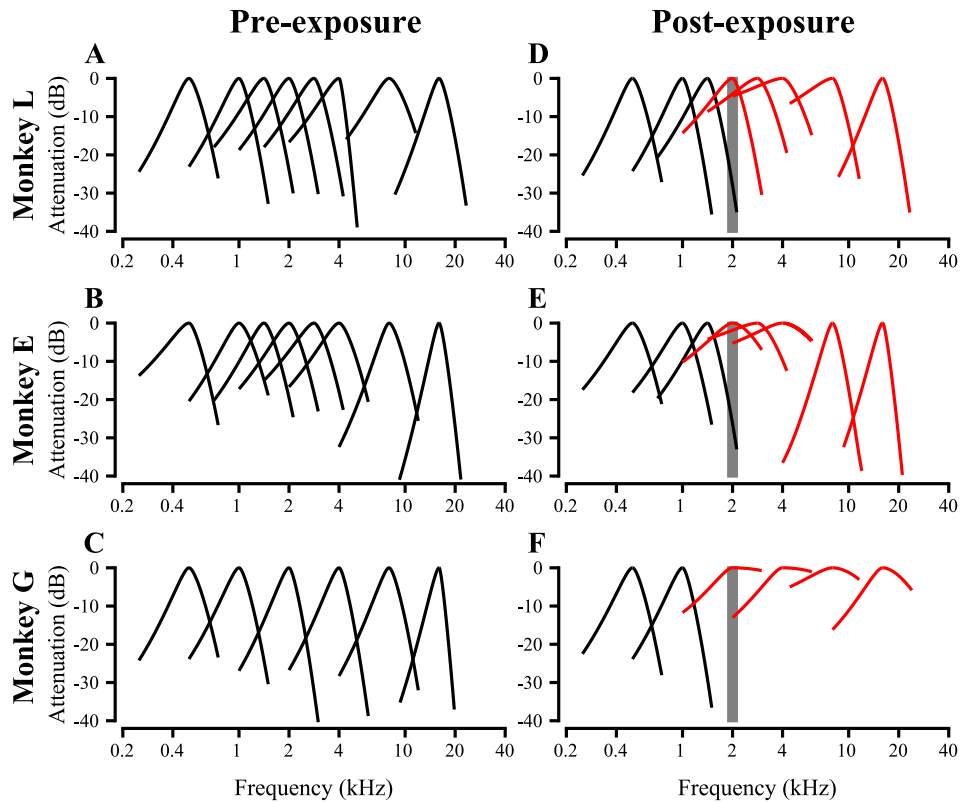
Fig. 4. Asymmetric auditory filters across the macaque audible frequency range. A–C: Pre-exposure filters estimated for Monkey L, E, and G, respectively. D–F: Post-exposure filters estimated for Monkey L, E, and G, respectively. Filters for frequencies below the noise exposure band are shown in black (0.5–1.414 kHz). Filters for frequencies at and above the noise exposure band are shown in red (2–16 kHz). Gray bars illustrate the spectral range of the noise exposure stimulus. (For interpretation of the references to color in this figure legend, the reader is referred to the web version of this article.)

Table 1.
ERB values (in Hz) of asymmetric auditory filters for a cohort of normal hearing macaques and for Monkey L, Monkey E, and Monkey G before and after noise exposure.

Frequency (kHz)	Mean (stdev) normative erb values	Monkey L ERB Values		Monkey E ERB Values		Monkey G ERB Values	
		pre-exposure	post-exposure	pre-exposure	post-exposure	pre-exposure	post-exposure
0.5	133.1 (15.22)	124.7	120.9	160.5	156.0	130.7	125.6
1	246.2 (25.54)	234.7	222.9	305.6	282.4	237.7	222.5
1.414	390.3 (8.34)	384.7	342.6	391.2	357.3	–	–
2	483.8 (64.83)	532.5	606.1	607.4	1173.0	405.5	3296.7
2.828	735.8 (105.3)	762.9	1243.1	918.6	1961.5	–	–
4	1002.2 (182.8)	895.7	2539.1	1283.9	3410.4	825.5	5548.0
8	1932.8 (393.0)	2693.8	3364.9	1799.8	1389.8	1729.6	7229.4
16	2491.3 (425.2)	3023.2	3189.1	2067.9	2218.5	1947.1	8869.6

Table 2.
One-sample *t*-tests comparing post-exposure *ERB* values for Monkey L, Monkey E, and Monkey G to mean *ERB* values from a normal hearing cohort (including pre-exposure values for Monkeys L, E, and G).

Frequency (kHz)	df (n-1)	Monkey L		Monkey E		Monkey G	
		t	p-value	t	p-value	t	p-value
0.5	5	−1.96	0.1078	3.68	0.0142	−1.20	0.2839
1	7	−2.58	0.0365	4.00	0.00518	−2.63	0.0338
1.414	4	−12.80	0.00022**	−8.86	0.00090*	–	–
2	7	5.34	0.00108*	30.07	0.00001***	122.73	0.00001***
2.828	6	12.75	0.00001***	30.80	0.00001***	–	–
4	7	23.79	0.00001***	37.26	0.00001***	70.33	0.00001***
8	7	10.31	0.00002***	−3.91	0.005831	38.12	0.00001***
16	7	4.64	0.00237	−1.82	0.1124	42.43	0.00001***

* significant at $p < 0.05$ level after Bonferroni correction to $p = 0.0023$.
** significant at $p < 0.01$ level after Bonferroni correction to $p = 4.55 \cdot 10^{-4}$.
*** significant at $p < 0.001$ level after Bonferroni correction to $p = 4.55 \cdot 10^{-5}$.
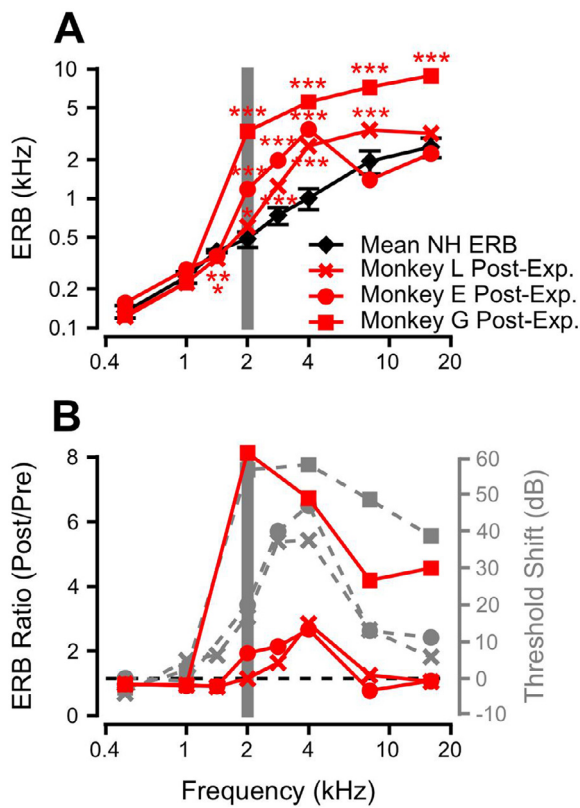
Fig. 5. Filter bandwidth estimates. A: Equivalent rectangular bandwidth (*ERB*) as a function of frequency. Mean data (± one standard deviation) for pre-exposure and control macaques (◇) and post-exposure data for Monkey L (×), Monkey E (○), and Monkey G (□). Post-exposure *ERB* values that significantly differed from mean control values are marked with asterisks (see Table 2 for statistics). B: *ERB* ratio (post-exposure/pre-exposure, red) as a function of frequency for Monkey L (×), Monkey E (○), and Monkey G (□). The horizontal dashed line represents an *ERB* ratio of 1, and indicates equal pre- and post-exposure *ERB* values. Early post-exposure audiometric threshold shifts for each subject (from Fig. 1A) are plotted in gray for comparison with the same symbol designations. Gray bars illustrate the spectral range of the noise exposure stimulus. (For interpretation of the references to color in this figure legend, the reader is referred to the web version of this article.)

3.3. Frequency selectivity as a function of hearing impairment

To further compare frequency selectivity and audiometric threshold shift, normalized *ERB* (ERB/f_0) was plotted as a function of absolute audiometric threshold (dB SPL) for each subject using pre- and early post-exposure values (Fig. 6A), after Glasberg and Moore (1986). Linear and nonlinear regressions were compared to determine the best fit. The relation between normalized *ERB* and audiometric threshold was best described by a one-term exponential function ($y = 0.2368 + 0.0086 * e^{(0.0836*x)}$; $R^2 = 0.885$, $p = 1.54 \times 10^{-19}$) according to the BIC, as shown by the solid black line.

The relation between *ERB* ratios (post-exposure/pre-exposure) and audiometric threshold shift was also best fit with a one-term exponential function (Fig. 6B; $y = 0.854 + 0.1166 * e^{(0.0698*x)}$; $R^2 = 0.889$, $p = 2.50e-9$) according to the BIC. The exponential relations in Fig. 6A and B show that frequency selectivity is relatively unaffected with up to approximately 30 dB of audiometric threshold shift, but degrades rapidly as thresholds rise above that value.

3.4. Audiometric threshold shift and frequency selectivity as a function of cochlear histopathology

Cochleas were extracted for histopathological analysis at various delays after the late post-exposure audiometric threshold shifts
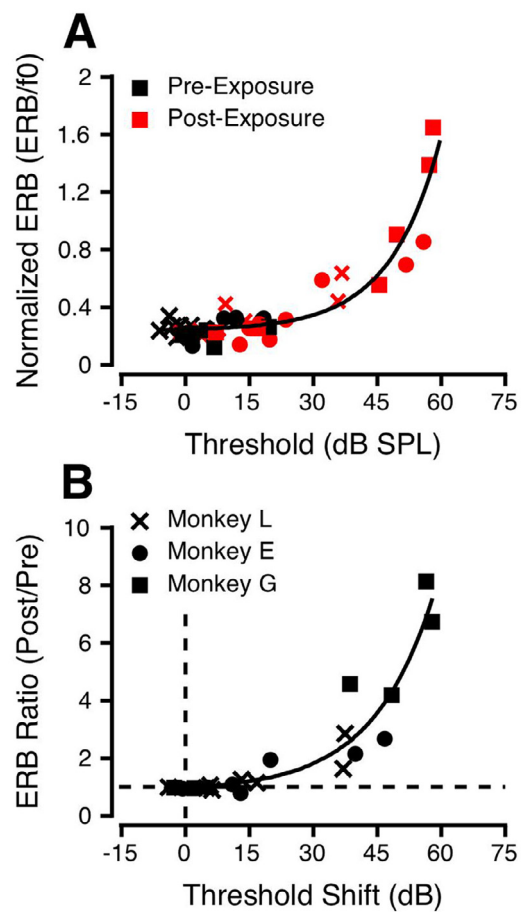
Fig. 6. Relationship between audiometric changes and changes in the bandwidth of perceptual filters. A: Normalized *ERB* ($ERB/f0$) as a function of absolute audiometric threshold (dB SPL) for Monkey L (×), Monkey E (○), and Monkey G (□), pre-exposure (black) and post-exposure (red; early post-exposure timepoint). The solid black line is a single exponential fit to all data points ($y = 0.2368 + 0.0086 * e^{(0.0483*x)}$). B: *ERB* ratio (post-exposure ERB/pre-exposure ERB) as a function of audiometric threshold shift (early post-exposure – pre-exposure) for Monkey L (×), Monkey E (○), and Monkey G (□). The horizontal dashed line indicates an *ERB* ratio of 1 (equal pre- and post-exposure *ERB* values). The vertical dashed line indicates a threshold shift of 0 (equivalent pre- and post-exposure audiometric thresholds). The solid black line is a single exponential fit to all data points ($y = 0.854 + 0.117 * e^{(0.0698*x)}$). (For interpretation of the references to color in this figure legend, the reader is referred to the web version of this article.)

in Fig. 1B (for details, see Section 2.2.1). As expected, hair cell loss was more extensive among OHCs than IHCs, and was worse at high-frequency regions (above the exposure band) than below (Fig. 7). The loss of IHC ribbon synapses extended a bit further apically than the loss of IHCs (Fig. 7B", C"). However, all three survival metrics in each ear followed similar apical-basal patterns. The degree of lesion asymmetry between the two ears was unexpectedly large for two of the subjects. Nevertheless, since the behavioral measures were obtained free-field, we elected to average the histopathological metrics across both ears of each animal. This approach is supported by several studies reporting that binaural thresholds are lower than monaural thresholds, implying binaural summation during signal detection (e.g. Gage, 1932; Shaw et al., 1947; Hirsch, 1948; Pollack, 1948; Hempstock et al., 1966; Heil, 2014) as opposed to listening with the "better ear". Consistent with this, the regression and mixed effects analyses that were conducted using the "better ear" or the "poorer ear" histological data generally resulted in poorer, often non-significant models (data not shown).
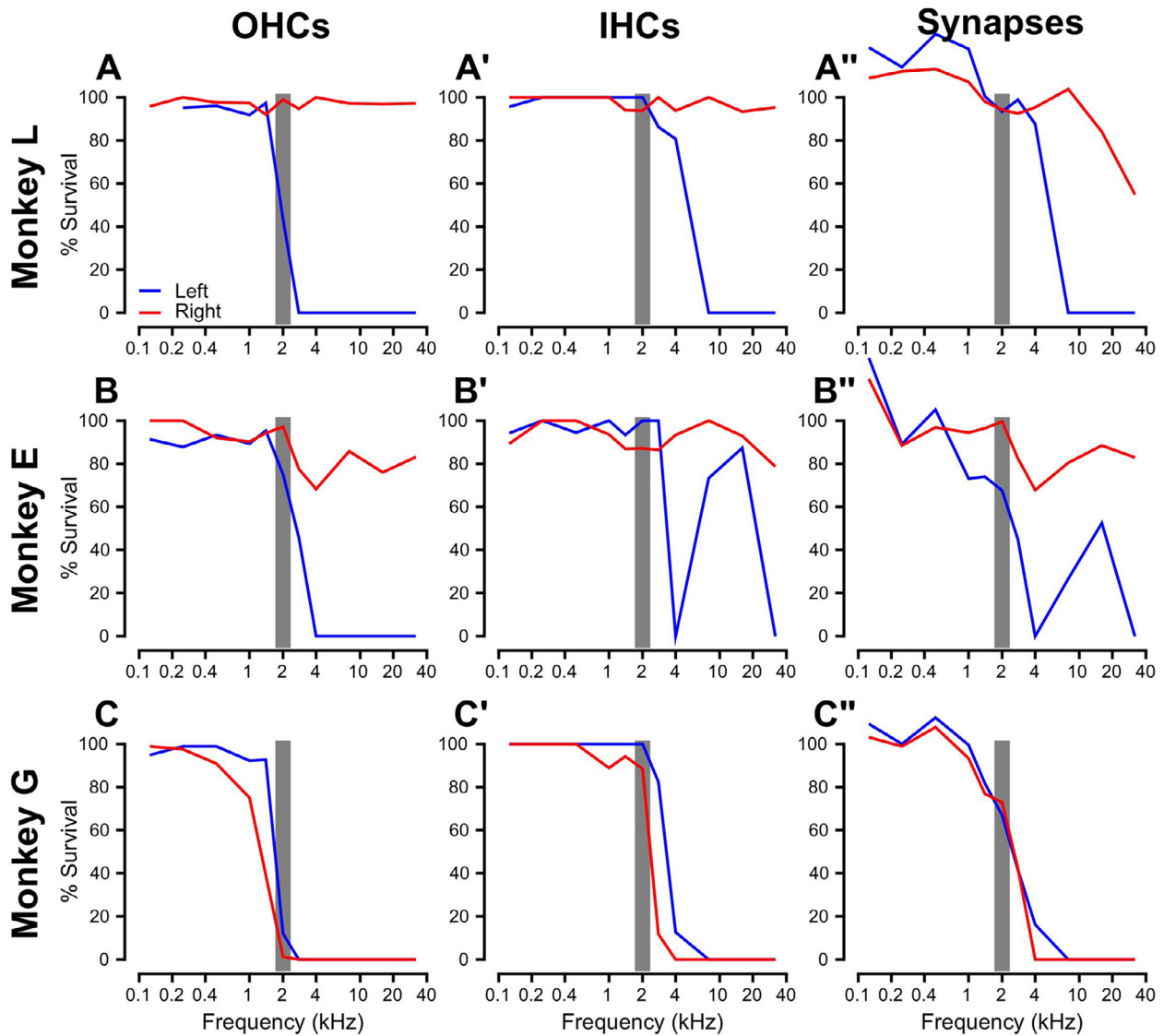
Fig. 7. Percentage survival of outer hair cells (A, B, C), inner hair cells (A', B', C'), and ribbon synapses (A", B", C") as a function of cochlear frequency place for each of the noise-exposed monkeys. Data are shown for each subject (Monkey L: A-A"; Monkey E: B-B"; Monkey G: C-C") with separate traces for the left ear (blue) and right ear (red). Gray bars illustrate the spectral range of the noise exposure stimulus. (For interpretation of the references to color in this figure legend, the reader is referred to the web version of this article.)
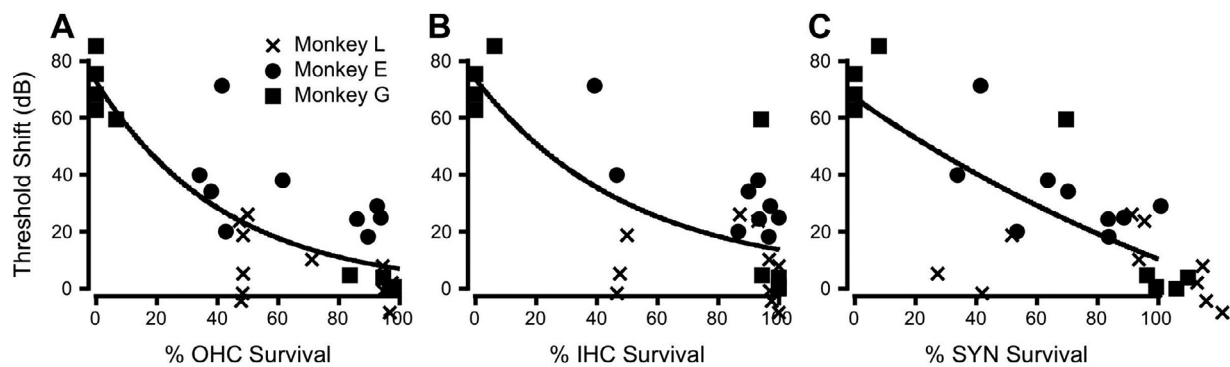
Fig. 8. Relationship between audiometric threshold shift and cochlear histopathology. A: Late post-exposure audiometric threshold shift as a function of outer hair cell survival at each corresponding signal/cochlear frequency place for Monkey L ($\times$), Monkey E ($\circ$), and Monkey G ($\square$). The solid black line is a one term exponential fit to all data points ($y = 0.0095 + 72.71*\exp(x*(-0.0236))$). B: Same as in A, but for inner hair cell survival. Data are fit with a one term exponential function ($y = 4.128 + 69.54*\exp(x*(-0.0199))$). C: Same as in A and B, but for ribbon synapse survival. Data are fit with a one term exponential function ($y = -63.19 + 130.11*\exp(x*(-0.0057))$).
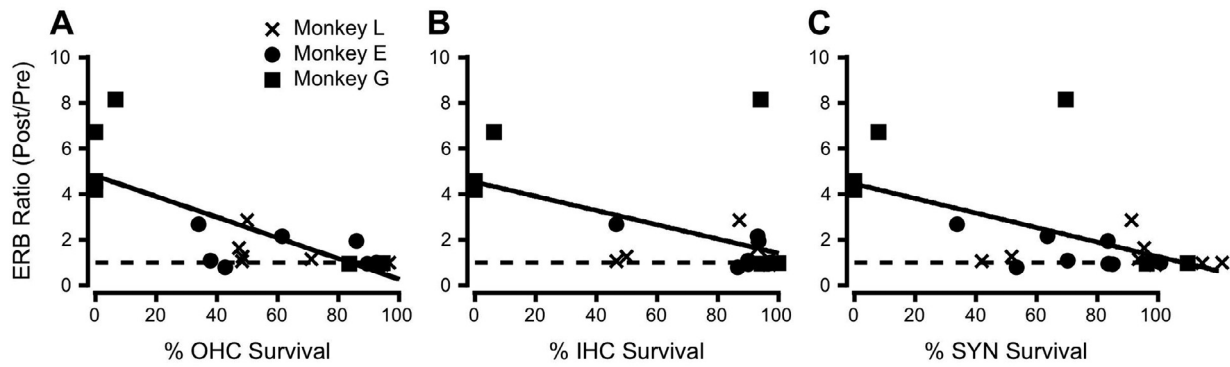
Fig. 9. Relationship between frequency selectivity and cochlear histopathology. A: *ERB* ratio as a function of outer hair cell survival at each corresponding signal/cochlear frequency place for Monkey L (×), Monkey E (○), and Monkey G (□). The solid black line is a linear fit to all data points ($y = 4.7965 + x*(-0.045429)$). An *ERB* ratio of 1 (horizontal dashed line) indicates equivalent pre- and post-exposure *ERB* values. B: Same as in A, but for inner hair cell survival. Data are fit with a linear function ($y = 4.5207 + x*(-0.03125)$). C: Same as in A and B, but for ribbon synapse survival. Data are fit with a linear function ($y = 4.4397 + x*(-0.031949)$).

Table 3A.
Stepwise multivariate linear regression model for describing audiometric threshold shift as a function of frequency and mean OHC, IHC, and ribbon synapse survival.
Without Interactions: Threshold Shift ~ 1 + OHC.

Term	Coefficient	*p*-value
Intercept	61.641	1.76e-10
OHC	−0.61654	3.24e-07

Fig. 8 shows the relations between late post-exposure audiometric threshold shifts and each histopathological metric at the appropriate cochlear place. As expected, threshold shifts were negatively correlated with all three metrics. According to the BIC, one-term exponential functions provided the best fit for mean survival of OHCs ($y = 0.0095 + 72.71 * e^{(-0.0236*x)}$; $R^2 = 0.701$, $p = 1.56e-07$), IHCs ($y = 4.128* + 69.54 * e^{(-0.0199*x)}$; $R^2 = 0.554$, $p = 2.76e-05$), and ribbon synapses ($y = -63.19* + 130.11 * e^{(-0.0057*x)}$; $R^2 = 0.586$, $p = 1.04e-05$). These models suggest that audiometric threshold shift increases exponentially with increasing severity of cochlear damage.

ERB ratio was also negatively correlated with survival of OHCs, IHCs, and ribbon synapses (Fig. 9). However, for this outcome measure, linear models provided the best fit for mean survival of OHCs ($y = 4.7965 + x*(-0.045429)$; $R^2 = 0.603$, $p = 2.13e-05$), IHCs ($y = 4.5207 + x*(-0.03125)$; $R^2 = 0.28$, $p = 0.011$), and ribbon synapses ($y = 4.4397 + x*(-0.031949)$; $R^2 = 0.326$, $p = 0.0055$). These models suggest that *ERB* ratio increases linearly with increasing severity of cochlear damage. Similar models were obtained for normalized *ERB* (data not shown). Considering the long and variable delay between behavioral testing and histological analysis, the observed correlations may underestimate the strength of this relationship.

Since many of these measures co-varied, stepwise multivariate linear regression was used to model their relative contributions to audiometric threshold shift (Table 3) and frequency selectivity (Table 4). Models contained frequency and mean OHC, IHC, and ribbon synapse survival as predictor variables, and either audiometric threshold shift (late post-exposure timepoint) or *ERB* ratio as the dependent variable. When excluding variable interactions, the models included OHC survival as a significant coefficient (see Tables 3A and 4A for coefficient statistics):

$$Threshold\ Shift\ \sim\ 1 + OHC\ \left(R^2\ =\ 0.626,\ p\ =\ 3.24e-07\right)$$

$$ERB\ Ratio\ \sim\ 1 + OHC + Frequency\ \left(R^2\ =\ 0.797,\ p\ =\ 2.67e-07\right)$$

Table 3B.
Stepwise multivariate linear regression model for describing audiometric threshold shift as a function of frequency and mean OHC, IHC, and ribbon synapse survival.
With Interactions: Threshold Shift ~ 1 + Frequency + OHC + IHC + Synapses + OHC*Frequency + IHC*Frequency + Synapses*Frequency + OHC*IHC + IHC*Synapses.

Term	Coefficient	*p*-value
Intercept	60.444	6.58e-05
Frequency	0.51428	0.38596
OHC	−5.1493	0.0045536
IHC	0.53219	0.031685
Synapses	2.5694	0.1508
OHC:Frequency	0.057208	0.045242
IHC:Frequency	−0.092825	0.0049246
Synapses:Frequency	0.067793	0.086125
OHC:IHC	0.050427	0.0071199
IHC:Synapses	−0.03513	0.055364

Table 4A.
Stepwise multivariate linear regression model for describing frequency selectivity as a function of frequency and mean OHC, IHC, and ribbon synapse survival.
Without Interactions: ERB Ratio ~ 1 + OHC + Frequency.

Term	Coefficient	*p*-value
Intercept	6.8806	1.46e-09
Frequency	−0.21248	0.00043
OHC	−0.064223	5.91e-08

Table 4B.
Stepwise multivariate linear regression model for describing frequency selectivity as a function of frequency and mean OHC, IHC, and ribbon synapse survival.
With Interactions: ERB Ratio ~ 1 + Frequency + OHC + IHC + Synapses + Synapses*IHC + Synapses*OHC + Synapses*Frequency + IHC*Frequency.

Term	Coefficient	*p*-value
Intercept	5.2072	1.30e-05
Frequency	−0.049711	0.46
OHC	−0.3574	1.29e-05
IHC	0.32491	5.31e-05
Synapses	−0.15587	0.0043
IHC:Frequency	−0.033111	7.60e-05
Synapses:Frequency	0.039443	0.00015
Synapses:OHC	0.0038163	9.07e-05
Synapses:IHC	−0.0023705	0.0015

However, when including interaction components, the models included several main effects and interaction terms (see Tables 3B and 4B for coefficient statistics):

$$Threshold\ Shift\ \sim\ 1 + Frequency + OHC + IHC + Synapses$$
$$+ OHC*Frequency + IHC*Frequency + Synapses*Frequency$$
$$+ OHC*IHC + IHC*Synapses\ \left(R^2\ =\ 0.893,\ p\ =\ 2.00\,e-07\right)$$

Table 5.

Comparing stepwise multivariate linear regression models with and without interactions for describing audiometric threshold shift and frequency selectivity as a function of frequency and mean OHC, IHC, and ribbon synapse survival.

Stepwise linear regression model	Audiometric threshold shift			ERB ratio		
	R^2	p-value	BIC value	R^2	p-value	BIC value
Without Interactions	0.626	3.24e-07	250.48	0.797	2.67e-07	66.50
With Interactions	0.893	2.00e-07	241.14	0.953	2.2e-07	53.02

$$ERB\ Ratio \sim 1 + Frequency + OHC + IHC + Synapses$$
$$+ Synapses * IHC + Synapses * OHC + Synapses * Frequency$$
$$+ IHC * Frequency \left(R^2 = 0.953,\ p = 2.2e - 07\right)$$

Models including interaction terms provided higher R^2 values and were more favorable than the models excluding interaction terms according to the BIC values (see Table 5). It is important to note that the BIC aggressively penalizes models with a greater number of parameters in order to avoid overfitting. Overall, these models suggest that audiometric threshold shift and frequency selectivity may be primarily attributed to OHC loss, but additional variability may be determined by complex patterns of cochlear damage and interactions across cochlear components.

4. Discussion

These findings provide the first pre- and post-noise exposure, within-subject comparisons of auditory filter bandwidths in an animal model, along with post-exposure cochlear histological characterization. Due to the sophisticated behavioral capabilities of these subjects, hearing impaired macaques provide a valuable model system for investigating the mechanisms underlying the degradation of auditory performance following cochlear damage (Stebbins, 1982; Burton et al., 2019). The relationship between cochlear damage and auditory performance is expected to be complex, since perception is the product of many neurophysiological and computational processing steps. These investigations will help draw connections between the extensive literature on human psychoacoustics in the presence of hearing loss and physiological and anatomical investigations of animal auditory neuroscience.

4.1. Relationship between frequency selectivity and audiometric threshold following noise exposure

Macaque perceptual filter widths increased with increasing severity of NIHL, indicating poorer frequency selectivity with greater hearing impairment. Since the current study used an identical masker level for pre- and post-exposure measurements, differences in filter width cannot be attributed to differences in masking condition – a factor that often complicates comparisons between normal hearing and hearing-impaired listeners. These findings recapitulate numerous studies of auditory filters in humans with hearing impairment (e.g. Tyler et al., 1984; Glasberg and Moore, 1986; Peters and Moore, 1992; Leek and Summers, 1993; Bernstein and Oxenham, 2006; Hopkins and Moore, 2011; Desloge et al., 2012; Shen et al., 2019). Furthermore, this study provides additional evidence for a relationship between degree of hearing loss and perceptual filter bandwidth for losses beyond a mild hearing impairment. Although some previous studies (e.g. Glasberg and Moore, 1986; Laroche et al., 1992) have suggested using a linear fit for thresholds beyond a mild hearing loss (i.e. using a ~30 dB inflection point to delineate normal vs. impaired frequency selectivity), the current data and others (Dubno and Dirks, 1989; Shen et al., 2019) support an expo-

nential relationship. This exponential relationship may not have been apparent in the former studies because the data were collected at one tone frequency (1 kHz) across many subjects without regard to the frequency of greatest impairment (Glasberg and Moore, 1986; Laroche et al., 1992). The current data and that of Shen et al. (2019) was compiled across multiple signal frequencies and subjects. Further factors that may contribute to the different trends observed include the inclusion of ERB values greater than 1.0, as well as differences in species.

As demonstrated here and in many previous investigations, perceptual frequency selectivity is typically normal or near normal for audiometric thresholds up to 30–40 dB HL and variably impaired in subjects with more than a mild hearing loss (Ryan et al., 1979; Hall et al., 1984; Glasberg and Moore, 1986; Peters and Moore, 1992; Florentine, 1992; Laroche et al., 1992; Leek and Summers, 1993; Sommers and Humes, 1993; Moore, 1995; Hopkins and Moore, 2011; Desloge et al., 2012; Shen et al., 2019). Subsequently, auditory filter shapes are also highly variable across individuals with hearing impairment. For example, the low- and high- frequency sides of filters can be affected independently (Tyler et al., 1984), as was seen in the 8 kHz filter from Monkey L (see Fig. 4A and D). Additionally, measures of frequency selectivity can remain variable even when hearing thresholds (Lutman et al., 1991) or stimulus presentation level (Leek and Summers, 1993; Sommers and Humes, 1993; Florentine et al., 1980; Desloge et al., 2012) were accounted for, with filter widths ranging from normal to 4-5 times the normal bandwidth for thresholds of 50 dB HL (Pick et al., 1977).

4.2. Relationship between noise-induced audiometric threshold shift and cochlear histopathology

An inverse relationship between indices of cochlear histopathology and hearing sensitivity has consistently been observed (e.g. Schuknecht, 1955; Miller et al., 1963; Stebbins et al., 1979; Hauser et al., 2018). Several animal studies point to OHC loss as the primary determinant of the first 30–50 dB of hearing impairment (e.g. Ryan and Dallos, 1975; Hawkins et al., 1976; Stebbins et al., 1979; Hamernik et al., 1989), whereas fractional IHC loss and selective ribbon synapse loss (i.e. synaptopathy) typically do not result in permanent threshold shifts (e.g. Lobarinas et al., 2013; Kujawa and Liberman, 2009; Liberman and Kujawa, 2017; Burton et al., 2018b). Liberman and Dodds (1984) report that both OHC and IHC damage can result in decreased sensitivity, but with distinct effects on other regions of the tuning curve. However, audiometric thresholds remain variable and difficult to predict purely based on OHC or IHC survival counts (e.g. Clark and Bohne, 1978; Ward and Duvall, 1971; Hunter-Duvar and Bredberg, 1974; Hunter-Duvar and Elliott, 1972, 1973; Moody et al., 1978; Luz et al., 1973; Suga and Lindsay, 1976; Lonsbury-Martin et al., 1987; Ward and Duvall, 1971; Schuknecht and Gacek, 1993; Landegger et al., 2016). Stereocilia condition may be an important determinant of threshold shifts (Liberman and Dodds, 1984; Engström, 1984; Wang et al., 2002), since surviving hair cells are often severely compromised. Unfortunately, we have not yet developed methods to assess stere-

ocilia condition in cochleas also prepared for counting ribbon synapses and hair cells.

The current data and stepwise multivariate linear regression modeling suggest that, while OHC damage plays a predominant role in determining audiometric threshold, interactions among cochlear structures may also contribute to the variability observed in previous work. While ribbon synapse loss alone is not known to cause audiometric threshold shifts (i.e. hidden hearing loss), the accumulation of additional cases and types of cochlear pathologies alongside immunohistochemical quantification of multiple cochlear components could improve understanding of the relationship between audiometric threshold shift and bilateral OHC, IHC, and ribbon synapse loss.

Finally, a high degree of inter-subject and across-ear variability was observed in degree of noise-induced audiometric threshold shift and cochlear damage. Inter-subject differences in noise susceptibility have been reported previously (Bohne et al., 1999), and appear to be significantly greater for more genetically heterogeneous species (i.e. guinea pigs, nonhuman primates) compared to inbred mouse strains (Wang et al., 2002). However, a unique and unexpected finding in this study was the marked asymmetry in cochlear histopathology for two of the subjects. This contrasts with studies that suggest a high degree of within-subject across-ear symmetry (Bohne et al., 1999), but is consistent with reports of differential susceptibility between ears in humans (Chung et al., 1983; Landegger et al., 2016).

4.3. Relationship between noise-induced changes in perceptual frequency selectivity and cochlear histopathology

In the current study, little or no change in frequency selectivity was observed at frequencies with very little or no OHC, IHC, or ribbon synapse loss. Frequency selectivity degraded with increasing damage; in particular, OHC survival seemed to be a large contributor to auditory filter width. Previous work by Smith et al. (1987) showed impaired psychophysical tuning curves in patas monkeys with selective damage to outer hair cells. Taken together, these data are consistent with the idea that the active mechanism of the OHCs is a predictor of both the absolute sensitivity and frequency selectivity of the normal cochlea, as has been previously suggested (Glasberg and Moore, 1986). These data are also consistent with reports that OHC loss is a major contributor to the first 30–40 dB of permanent hearing loss (Saunders et al., 1991).

Individual differences in frequency selectivity of hearing-impaired subjects may be explained in part by differences in underlying pathology. Even when the etiology of hearing loss is matched (e.g. noise-induced), filter widths may still be significantly variable for a given degree of threshold elevation (Laroche et al., 1992). This variability may be accounted for by the interaction components identified in the stepwise multivariate linear regression model. For example, frequency selectivity may be even broader when there is both OHC and ribbon synapse loss (i.e. OHC*Synapses interaction), as compared to OHC loss alone. Evaluation of stereocilia condition may provide additional predictive power (Liberman and Dodds, 1984) and should be assessed in future studies.

The relationship between cochlear damage and perceptual frequency selectivity remains highly variable, even in controlled animal studies (Ryan et al., 1979; Nienhuys and Clark, 1979; Marean et al., 1998). These three studies examined changes in frequency selectivity as measured by psychophysical tuning curves (Ryan et al., 1979) or auditory filter widths (Nienhuys and Clark, 1979; Marean et al., 1998) before and after ototoxic kanamycin treatment in animal models. Ryan et al. (1979) observed variable elevation of tuning curve thresholds, loss of tuning curve tips, and slight broadening of tuning curve widths in chinchillas with greater than 50 dB of hearing loss, which was typically associated with combined OHC and IHC loss. Similarly, Neinhuys and Clark (1979) found that filter bandwidths were unaffected in kanamycin-treated cats, even in the presence of complete OHC loss in the implicated frequency regions, unless IHC loss also exceeded 40%, providing further support for a model including interaction components. Finally, changes in notched-noise derived auditory filter width correlated with audiometric threshold shift in kanamycin-treated starlings (Marean et al., 1998), which exhibit mixed OHC and IHC loss. These correlations persisted throughout the course of kanamycin treatment and audiometric threshold recovery following hair cell regeneration. Given that estimates of perceptual frequency selectivity vary with methodology (e.g. Glasberg et al., 1984a; Eustaquio-Martin and Lopez-Poveda, 2011), methodological differences should be noted and comparisons with the present study should be made with caution. While differences in species and methods of hearing loss induction also make comparisons difficult, these studies are still instructive for interpreting the present results, as they support a model in which perceptual frequency selectivity is determined by survival of multiple cochlear structures. This multivariate relationship was strongly supported in the current study ($R^2 = 0.953$), despite the long time delay (~4-18 months) between behavioral data collection and cochlear histopathological characterization that varied across subjects. The authors predict that the model could even be strengthened if the time delay was minimized.

4.4. Future directions: frequency selectivity in other noise-induced cochlear pathologies

The approach of the present study could be extended to assess the relationship between cochlear histopathology and auditory perception in other pathologies. Recent investigations of noise-induced temporary threshold shifts (TTS) reveal that IHC ribbon synapse loss occurs prior to the OHC loss that is typically associated with permanent NIHL (Kujawa and Liberman, 2009; Valero et al., 2017). Though TTS-induced synapse loss, or synaptopathy, does not result in decreased hearing sensitivity, it is suspected to affect suprathreshold auditory processing (e.g. Bharadwaj et al., 2014; Plack et al., 2014; Oxenham, 2016). Frequency selectivity following TTS and the associated sub-clinical damage to the auditory periphery is not well-described. In a study of noise-exposed industrial workers, Bergman et al. (1992) found variable changes in frequency selectivity estimates accompanied by equally variable TTS after a work day. Acute TTS in humans also worsens frequency selectivity in noise-exposed normal hearing subjects (Feth et al., 1979; Klein and Mills, 1981). However, the impaired frequency selectivity reported in these studies is likely dominated by reversible damage to OHCs during the TTS. Broader auditory filters and impaired frequency selectivity have been reported for normal hearing participants with impaired speech-in-noise perception, some of whom likely experienced synaptopathy subsequent to TTS (Pick and Evans, 1983; Badri et al., 2011). Contributions from OHC loss cannot be ruled out in this study either, since many participants had subclinical audiometric notches and poorer extended high frequency thresholds compared to controls. Future studies examining frequency selectivity in animal models of synaptopathy could provide key evidence for distinguishing the contributions of specific cochlear components to impaired frequency selectivity and establishing appropriate therapeutic targets. These studies would also help establish the clinical utility of new methods for acquiring auditory filters, which may be both clinically feasible and sensitive to different hearing impairments (Shen et al., 2014, 2019).

Declaration of Competing Interest

The authors declare that they have no conflicts of interest.

Acknowledgments

References

Badri, R., Siegel, J.H., Wright, B.A., 2011. Auditory filter shapes and high-frequency hearing in adults who have impaired speech in noise performance despite clinically normal audiograms. J. Acoust. Soc. Am. 129 (2), 852–863.

Bergman, M., Najenson, T., Korn, C., Harel, N., Erenthal, P., Sachartov, E., 1992. Frequency selectivity as a potential measure of noise damage susceptibility. Br. J. Audiol. 26 (1), 15–22.

Bernstein, J.G.W., Oxenham, A.J., 2006. The relationship between frequency selectivity and pitch discrimination: sensorineural hearing loss. J. Acoust. Soc. Am. 120 (6), 3929–3945.

Bharadwaj, H.M., Verhulst, S., Shaheen, L, Liberman, M.C., Shinn-Cunningham, B.G., 2014. Cochlear neuropathy and the coding of supra-threshold sound. Front. Syst. Neurosci. 8 (26), 1–17.

Bohlen, P., Dylla, M., Timms, C., Ramachandran, R., 2014. Detection of modulated tones in modulated noise by non-human primates. JARO 15, 801–821.

Bohne, B.A., Harding, G.W., Nordmann, A.S., Tseng, C.J., Liang, G.E., Bahadori, R.S., 1999. Survival-fixation of the cochlea: a technique for following time-dependent degeneration and repair in noise-exposed chinchillas. Hear. Res. 134, 163–178.

Burton, J.A., Dylla, M.E., Ramachandran, R., 2018a. Frequency selectivity in macaque monkeys measured using a notched-noise method. Hear. Res. 357, 73–80.

Burton, J.A., McCrate, J., Hauser, S., Mackey, C., Feller, J., Ramachandran, R., 2018b. Temporal and spectral resolution in a nonhuman primate model of noise-induced hearing loss. Poster presented at the Auditory System Gordon Research Conference.

Burton, J.A., Valero, M.D., Hackett, T.A., Ramachandran, R., 2019. The use of nonhuman primates in studies of noise injury and treatment. J. Acoust. Soc. Am. 146 (5), 3770–3789.

Chung, D.Y., Willson, G.N., Gannon, R.P., 1983. Lateral differences in susceptibility to noise damage. Audiology 22 (2), 199–205.

Clark, W.W., Bohne, B.A., 1978. Animal model for the 4-kHz tonal dip. Ann. Otol. Rhinol. Laryngol. 87 (4 Pt 2 Suppl 51), 1–16.

Desloge, J.G., Reed, C.M., Braida, L.D., Perez, Z.D., Delhorne, L.A., 2012. Auditory-filter characteristics for listeners with real and simulated hearing impairment. Trends Amplif. 16 (1), 19–39.

Dubno, J.R., Dirks, D.D., 1989. Auditory filter characteristics and consonant recognition for hearing-impaired listeners. J. Acoust. Soc. Am. 85 (4), 1666–1675.

Dylla, M., Hrnicek, A., Rice, C., Ramachandran, R., 2013. Detection of tones and their modification by noise in nonhuman primates. JARO 14, 547–560.

Engström, B., 1984. Fusion of stereocilia on inner hair cells in man and in the rabbit, rat and guinea pig. Scand. Audiol. 13, 87–92.

Eustaquio-Martin, A., Lopez-Poveda, E.A., 2011. Isoresponse versus isoinput estimates of cochlear filter tuning. J. Assoc. Res. Otolaryngol. 12 (3), 281–299.

Feth, L.L., Oesterle, E.C., Kidd, G., 1979. Frequency selectivity after noise exposure. J. Acoust. Soc. Am. 65, S118.

Fernandez, K.A., Jeffers, P.W., Lall, K., Liberman, M.C., Kujawa, S.G., 2015. Aging after noise exposure: acceleration of cochlear synaptopathy in "recovered" ears. J. Neurosci. 35 (19), 7509–7520.

Florentine, M., 1992. Effects of cochlear impairment and equivalent-threshold masking on psychoacoustic tuning curves. Audiology 31, 241–253.

Florentine, M., Buus, S., Scharf, B., Zwicker, E., 1980. Frequency selectivity in normally-hearing and hearing-impaired observers. J. Speech Hear. Res. 23, 646–669.

Gage, F.H., 1932. A note on the binaural threshold. Br. J. Psychol. 23 (2), 148.

Gates, G.A., Schmid, P., Kujawa, S.G., Nam, B.H., D'Agostino, R., 2000. Longitudinal threshold changes in older men with audiometric notches. Hear. Res. 141 (1-2), 220–228.

Gelfand, S.A., 2009. Essentials of Audiology, 3. ed. Thieme Medical Publishers, New York, NY.

Glasberg, B.R., Moore, B.C.J., 1986. Auditory filter shapes in subjects with unilateral and bilateral cochlear impairments. J. Acoust. Soc. Am. 79 (4), 1020–1033.

Glasberg, B.R., Moore, B.C.J., Nimmo-Smith, I., 1984a. Comparison of auditory filter shapes derived with three different maskers. J. Acoust. Soc. Am. 75 (2), 536–544.

Glasberg, B.R., Moore, B.C.J., Patterson, R.D., Nimmo-Smith, I., 1984b. Dynamic range and asymmetry of the auditory filter. J. Acoust. Soc. Am. 76 (2), 419–427.

Greenwood, D.D., 1990. A cochlear frequency-position function for several species – 29 years later. J. Acoust. Soc. Am. 87 (6), 2591–2605.

Hall, J.W., Grose, J.H., 1989. Spectrotemporal analysis and cochlear hearing impairment: effects of frequency selectivity, temporal resolution, signal frequency, and rate of modulation. J. Acoust. Soc. Am. 85 (6), 2550–2562.

Hall, J.W., Tyler, R.S., Fernandes, M.A., 1984. Factors influencing the masking level difference in cochlear hearing-impaired and normal-hearing listeners. J. Speech Hear. Res. 27, 145–154.

Hamernik, R.P., Patterson, J.H., Turrentine, G.A., Ahroon, W.A., 1989. The quantitative relation between sensory cell loss and hearing thresholds. Hear. Res. 38, 199–212.

Hauser, S.N., Burton, J.A., Mercer, E.T., Ramachandran, R., 2018. Effects of noise overexposure on tone detection in noise in nonhuman primates. Hear. Res. 357, 33–45.

Hawkins, J.E., Johnsson, L.-G., Stebbins, W.C., Moody, D.B., Coombs, S.L., 1976. Hearing loss and cochlear pathology in monkeys after noise exposure. Acta Otolaryngol. 81, 337–343.

Heil, P., 2014. Towards a unifying basis of auditory thresholds: binaural summation. JARO 15 (2), 219–234.

Hempstock, T.I., Bryan, M.E., Webster, J.B.C., 1966. Free field threshold variance. J. Sound Vib. 4, 33–44.

Hirsch, I. J., 1948. Binaural summation-a century of investigation. Psychol. Bull. 45 (3), 193.

Hopkins, K., Moore, B.C.J., 2011. The effects of age and cochlear hearing loss on temporal fine structure sensitivity, frequency selectivity, and speech reception in noise. J. Acoust. Soc. Am. 130 (1), 334–349.

Hunter-Duvar, I.M., Bredberg, G., 1974. Effects of intense auditory stimulation: hearing losses and inner ear changes in the chinchilla. J. Acoust. Soc. Am. 55 (4), 795–801.

Hunter-Duvar, I.M., Elliott, D.N., 1972. Effects of intense auditory stimulation: hearing losses and inner ear changes in the squirrel monkey. J. Acoust. Soc. Am. 52 (4), 1181–1192.

Hunter-Duvar, I.M., Elliott, D.N., 1973. Effects of intense auditory stimulation: hearing losses and inner ear changes in the squirrel monkey. II. J. Acoust. Soc. Am. 54 (5), 1179–1183.

Klein, A.J., Mills, J.H., 1981. Physiological and psychophysical measures from humans with temporary threshold shift. J. Acoust. Soc. Am. 70 (4), 1045–1053.

Kujawa, S.G., Liberman, M.C., 2009. Adding insult to injury: Cochlear nerve degeneration after "temporary" noise-induced hearing loss. J. Neurosci. 29 (45), 14077–14085.

Landegger, L.D., Psaltis, D., Stankovic, K.M., 2016. Human audiometric thresholds do not predict specific cellular damage in the inner ear. Hear. Res. 335, 83–93.

Laroche, C., Hétu, R., Quoc, H.T., Josserand, B., Glasberg, B., 1992. Frequency selectivity in workers with noise-induced hearing loss. Hear. Res. 64, 61–72.

Leek, M.R., Summers, V., 1993. Auditory filter shapes of normal-hearing and hearing-impaired listeners in continuous broadband noise. J. Acoust. Soc. Am. 94 (6), 3127–3137.

Liberman, M.C., Dodds, L.W., 1984. Single-neuron labeling and chronic cochlear pathology. III. Stereocilia damage and alterations of threshold tuning curves. Hear. Res. 16, 55–74.

Liberman, M.C., Kujawa, S.G., 2017. Cochlear synaptopathy in acquired sensorineural hearing loss: manifestations and mechanisms. Hear. Res. 349, 138–147.

Lobarinas, E., Salvi, R., Ding, D., 2013. Insensitivity of the audiogram to carboplatin induced inner hair cell loss in chinchillas. Hear. Res. 302, 113–120.

Lonsbury-Martin, B.L., Martin, G.K., Bohne, B.A., 1987. Repeated TTS exposures in monkeys: alterations in hearing, cochlear structure, and single-unit thresholds. J. Acoust. Soc. Am. 81 (5), 1507–1518.

Lutman, M.E., Gatehouse, S., Worthington, A.G., 1991. Frequency resolution as a function of hearing threshold level and age. J. Acoust. Soc. Am. 89 (1), 320–328.

Luz, G.A., Mosko, J.D., Fletcher, J.L., Fravel, W.J., 1973. The relation between temporary threshold shift and permanent threshold shift in rhesus monkeys exposed to impulse noise. Acta Otolaryngol. 76 (Sup312), 5–15.

Macmillan, N. A., Creelman, C. D., 2005. Detection Theory: A User's guide., 2nd Ed Lawrence Erlbaum Associates, Mahwah, NJ.

Marean, G.C., Burt, J.M., Beecher, M.D., Rubel, E.W., 1998. Auditory perception following hair cell regeneration in European starling (Sturnus vulgaris): frequency and temporal resolution. J. Acoust. Soc. Am. 103 (6), 3567–3580.

Miller, J.D., Watson, C.S., Covell, W.P., 1963. Deafening effects of noise on the cat. Acta Otolaryngol. Suppl. 176, 1–84.

Moody, D.B., Stebbins, W.C., Hawkins, J.E., Johnsson, L.-G., 1978. Hearing loss and cochlear pathology in the monkey (Macaca) following exposure to high levels of noise. Arch. Oto-Rhino-Laryng. 220, 47–72.

Moore, B.C.J., 1995. Perceptual consequences of cochlear hearing loss and their implications for the design of hearing aids. Ear Hear. 17 (2), 133–161.

Moore, B.C.J., 1985. Frequency selectivity and temporal resolution in normal and hearing-impaired listeners. Br. J. Audiol. 19, 189–201.

Moore, B. C. J., Glasberg, B. R., 1987. Formulae describing frequency selectivity as a function of frequency and level, and their use in calculating excitation patterns. Hear. Res. 28, 209–225.

Nienhuys, T.G.W., Clark, G.M., 1979. Critical bands following the selective destruction of cochlear inner and outer hair cells. Acta Otolaryngol. 88, 350–358.

Niemiec, A.J., Yost, W.A., Shofner, W.P., 1992. Behavioral measures of frequency selectivity in the chinchilla. J. Acoust. Soc. Am. 92 (5), 2636–2649.

Osmanski, M.S., Song, X., Wang, X., 2013. The role of harmonic resolvability in pitch perception in a vocal nonhuman primate, the common marmoset (Callithrix jacchus). J. Neurosci. 33 (21), 9161–9168.

Oxenham, A.J., 2016. Predicting the perceptual consequences of hidden hearing loss. Trends Hear. 20, 1–6.

Patterson, R.D., Nimmo-Smith, I., 1980. Off-frequency listening and auditory filter asymmetry. J. Acoust. Soc. Am. 67 (1), 229–245.

Peters, R.W., Moore, B.C.J., 1992. Auditory filter shapes at low center frequencies in young and elderly hearing-impaired subjects. J. Acoust. Soc. Am. 91 (1), 256–266.

Pfingst, B.E., Laycock, J., Flammino, F., Lonsbury-Martin, B., Martin, G., 1978. Pure tone thresholds for the rhesus monkey. Hear Res. 1, 43–47.

Pick, G.F., Evans, E.F., 1983. Dissociation between frequency resolution and hearing threshold. In: Klinke, R., Hartmann, R. (Eds.), Hearing: Physiological Bases and Psychophysics. Springer-Verlag, Berlin, Germany, pp. 393–397.

Pick, G., Evans, E.F., Wilson, J.P., 1977. Frequency resolution in patients with hearing loss of cochlear origin. In: Evans, E.F., Wilson, J.P. (Eds.), *Psychophysics and Physiology of Hearing*. Academic Press, London, pp. 273–282.

Plack, C.J., Barker, D., Prendergast, G., 2014. Perceptual consequences of "hidden" hearing loss. Trends Hear. 18, 1–11.

Pollack, I., 1948. Monaural and binaural threshold sensitivity for tones and for white noise. J. Acoust. Soc. Am. 20, 52–57.

Radziwon, K.E., Sheppard, A., Salvi, R.J., 2019. Psychophysical changes in temporal processing in chinchillas with noise-induced hearing loss: a literature review. J. Acoust. Soc. Am. 146 (5), 3733–3742.

Reed, C.M., Braida, L.D., Zurek, P.M., 2009. Review of the literature on temporal resolution in listeners with cochlear hearing impairment: a critical assessment of the role of suprathreshold deficits. Trends Amplif. 13 (1), 4–43.

Ryan, A., Dallos, P., 1975. Effect of absence of cochlear outer hair cells on behavioural auditory threshold. Nature 253, 44–46.

Ryan, A., Dallos, P., McGee, T., 1979. Psychophysical tuning curves and auditory thresholds after hair cell damage in the chinchilla. J. Acoust. Soc. Am. 66 (2), 370–378.

Saunders, J.C., Cohen, Y.E., Szymko, Y.M., 1991. The structural and functional consequences of acoustic injury in the cochlea and peripheral auditory system: a five year update. J. Acoust. Soc. Am. 90 (1), 136–146.

Schuknecht, H.F., 1955. Presbycusis. Laryngoscope 65 (6), 402–419.

Schuknecht, H.F., Gacek, M.R., 1993. Cochlear pathology in presbycusis. Ann. Otol. Rhinol. Laryngol. 102, 1–16.

Shaw, W.A., Newman, E.B., Hirsh, I.J., 1947. The difference between monaural and binaural thresholds. J. Exp. Psychol. 37, 229–242.

Shen, Y., Kern, A.B., Richards, V.M., 2019. Toward routine assessment of auditory filter shape. JSLHR 62, 442–455.

Shen, Y., Sivakumar, R., Richards, V.M., 2014. Rapid estimation of high-parameter auditory filter shapes. J. Acoust. Soc. Am. 136 (4), 1857–1868.

Smith, D.W., Moody, D.B., Stebbins, W.C., Norat, M.A., 1987. Effects of outer hair cell loss on the frequency selectivity of the patas monkey auditory system. Hear. Res. 29, 125–138.

Sommers, M.S., Humes, L.E., 1993. Auditory filter shapes in normal-hearing, noise–masked normal, and elderly listeners. J. Acoust. Soc. Am. 93 (5), 2903–2914.

Stebbins, W.C., 1982. Concerning the need for more sophisticated animal models in sensory behavioral toxicology. Environ. Health Perspect. 44, 77–85.

Stebbins, W.C., Hawkins, J.E., Johnsson, L-G., Moody, D.B., 1979. Hearing thresholds with outer and inner hair cell loss. Am. J. Otolaryngol. 1 (1), 15–27.

Suga, F., Lindsay, J.R., 1976. Histopathological observations of presbycusis. Ann. Otol. 85, 169–184.

Tyler, R.S., Hall, J.W., Glasberg, B.R., Moore, B.C.J., Patterson, R.D., 1984. Auditory filter asymmetry in the hearing impaired. J. Acoust. Soc. Am. 76 (5), 1363–1368.

Valero, M.D., Burton, J.A., Hauser, S.N., Hackett, T.A., Ramachandran, R., Liberman, M.C., 2017. Noise-induced cochlear synaptopathy in rhesus monkeys (Macaca mulatta). Hear. Res. 353, 213–223.

Wang, Y., Hirose, K., Liberman, M.C., 2002. Dynamics of noise-induced cellular injury and repair in the mouse cochlea. JARO 3, 248–268.

Ward, W.D., Duvall, A.J., 1971. Behavioral and ultrastructural correlates of acoustic trauma. Ann. Otol. 80, 881–896.